Applied Catalysis B: Environmental 110 (2011) 195–206

Contents lists available at SciVerse ScienceDirect

Applied Catalysis B: Environmental

journal homepage: www.elsevier.com/locate/apcatb

Co-doping a metal (Cr, Fe, Co, Ni, Cu, Zn, Ce, and Zr) on Mn/TiO_2 catalyst and its effect on the selective reduction of NO with NH_3 at low-temperatures

Boningari Thirupathi, Panagiotis G. Smirniotis*

Chemical Engineering Program, School of Energy, Environmental, Biological and Medicinal Engineering, University of Cincinnati, Cincinnati, OH 45221-0012, USA

ARTICLE INFO

Article history:
Received 14 June 2011
Received in revised form 21 August 2011
Accepted 1 September 2011
Available online 8 September 2011

Keywords:
Low-temperature NH_3-SCR
Manganese oxide (MnO_x)
NO
XPS
In situ FTIR
Optimization for NO reduction

ABSTRACT

A series of Mn–M′/TiO_2 (M′ = Cr, Fe, Co, Ni, Cu, Zn, Ce, and Zr) catalysts were prepared using incipient wetness technique and investigated for the low-temperature selective catalytic reduction (SCR) of NO with ammonia in the presence of excess oxygen. A combination of various physico-chemical techniques was used to investigate the influence of co-doped metals on the characteristics of Mn/TiO_2 catalyst. The catalytic performance of these materials was compared with respect to the M′/Mn atomic ratio in order to examine the correlation between physicochemical characteristics and reactivity of optimized materials. XRD results suggest that metal oxide species exist in a highly dispersed state at a certain level called two-dimensional monolayer coverage. Our XPS results illustrated that the MnO_2 phase is extremely dominant over the Mn_2O_3 phase (Mn^{4+}/Mn^{3+} = 22.31, 96%) in the Mn–Ni(0.4)/TiO_2 anatase catalyst, whereas Mn_2O_3 phase is in competition with MnO_2 in other catalysts (Mn^{4+}/Mn^{3+} = 1.34–12.67). H_2-TPR data results are in good accordance with XPS results that the absence of the high-temperature (736 K) peak indicates that the dominant phase is MnO_2 in Mn–Ni(0.4)/TiO_2 catalyst. This increase in reducibility of manganese and dominant MnO_2 phase seems to be the reason for the superior activity and time on stream patterns of our best catalyst. BET and pore volume measurements revealed high surface area and pore volume of the Mn–Ni/TiO_2 catalyst. The *in situ* NH_3-FTIR results suggest that the manganese (Mn/TiO_2) and manganese–nickel (Mn–Ni/TiO_2) surface sites have only Lewis acidity, with no apparent Brönsted acidity. The catalytic performance of various Mn–M′/TiO_2 (M′/Mn = 0, 0.2, 0.4, 0.6, 0.8) catalysts was studied for the low-temperature SCR reaction at a range of temperatures (160–240 °C) under industrial conditions using GHSV = 50,000 h^{-1}. The intrinsic activity of Mn–Ni/TiO_2 catalyst with M′/Mn = 0.4 atomic ratio measured under differential reaction conditions, was found to be highly active, selective and broadening the temperature window for this reaction.

Published by Elsevier B.V.

1. Introduction

Usually, transition metal oxides show good SCR activity in the low temperature range, such as V_2O5/TiO_2–SiO_2–MoO_3 [1], Cr/TiO_2 [2], Mn/TiO_2 [3], Fe_xTiO_y [4], Co/TiO_2, Ni/TiO_2 [5], Cu/TiO_2 [6]. Particularly, manganese-based catalysts have attracted much interest due to their unique redox properties which make them significant for a variety of applications. Thus, in recent years, manganese oxides have been proposed as catalysts for several applications such as the CO oxidation [7], selective reduction of nitrobenzene [8], CH_4 oxidation [9] and the selective catalytic reduction of NO with NH_3 [3,5,10]. Among the low-temperature SCR catalysts, manganese oxide-based catalysts have been proven to be the most active catalysts [3,5,10,11]. However, the SCR activity, broadening of temperature window and time on stream patterns of these catalysts still need to be improved. Doping cations (metals) can enhance NO conversion and N_2 selectivity of the manganese oxide-based catalysts in low-temperature NH_3-SCR [12].

In this paper, selected elements including Cr, Fe, Co, Ni, Cu, Zn, Zr, and Ce were co-doped into the Mn/TiO_2 catalyst. For each element we varied the M′/Mn atomic ratio of the co-dopant (M′) used in the range of 0–0.8 in order to optimize the content of co-dopant and to investigate the effect on SCR activity with respect to various temperatures (160–240 °C). Among all co-dopants used, Ni showed an impressive promoting effect for the Mn/TiO_2 catalyst. Based on these results, we further investigated the influence of M′ (co-dopant) addition on the M′–Mn/TiO_2 catalyst structure, crystalline phase transformation, reduction profile, acidity and catalytic activity using various physicochemical characterization techniques.

The specific surface manganese oxide phases and the high surface concentration of manganese are decisive important for the SCR performance of the metal oxide catalysts at low-temperatures [13]. Thus, the existence of surface manganese phase and surface atomic concentrations of each metal were investigated by the optimal

* Corresponding author. Tel.: +1 513 556 1474; fax: +1 513 556 3473.
E-mail address: panagiotis.smirniotis@uc.edu (P.G. Smirniotis).

0926-3373/$ – see front matter. Published by Elsevier B.V.
doi:10.1016/j.apcatb.2011.09.001

combination of Gaussian bands by the Mn 2p and Ni 2p deconvoluted XPS spectra. The reduction of NO takes place via a redox mechanism in which the rate determining step is oxygen removal from the metal oxide. Thus, the reducibility of metal oxide species appears to be one of the most crucial parameters that affect catalytic performance for the selective reduction of NO. The SCR activity correlates with the onset of reduction in temperature-programmed reduction (TPR) experiments, indicating a correlation between the SCR process and active surface oxygen. Hence, H_2-TPR was conducted to evaluate the variation of redox properties during the co-doping process. The *in situ* FTIR of NH_3 adsorption were carried out to reveal the evolution of total acidity and specific acidic sites present over the surface of the catalyst, which are fundamental for the SCR reaction.

2. Experimental

2.1. Catalysts preparation

A series of Mn–M′/TiO_2 (M′ = Cr, Fe, Co, Ni, Cu, Zn, Ce, and Zr) catalysts were prepared by adopting a wet-impregnation method. TiO_2 anatase (Hombikat UV 100 from Sachtleben Chemie) was used as support material to prepare these catalysts. Nitrates (Mn, Cr, Fe, Co, Ni, Cu, Zn, Ce), and oxy nitrates (Zr) were used as the precursors of manganese and co-metal oxides. The manganese loadings were selected as 5 wt.% and the co-metal loadings were varied ranging from 0 to 4 wt.% in each type. For this purpose, the required amounts of precursors were added to a 100 mL beaker containing 1.0 g of support in 50 mL deionized water. The excess water was then slowly evaporated on a water bath with continuous stirring at 70 °C. For comparison purposes, TiO_2 anatase (Hombikat) support alone was mixed in deionized water, and then water was evaporated using a water bath with continuous heating and stirring. The resulting materials were oven dried at 120 °C for 12 h, and were ground and sieved (80–120 mesh) to obtain homogeneous powder. Prior to the reaction studies, the powder was calcined in a tubular oven at 400 °C for 2 h under continuous air flow (150 mL min^{-1}). The metal components of the catalysts are denoted as atomic ratios. The amount of manganese was kept constant (5 wt.%) and the amount of second metal varied. All the ratios of the catalysts in this study are M′/Mn = 0, 0.2, 0.4, 0.6, 0.8. For example, Mn–Ni(0.4)/TiO_2 indicates that the atomic ratio of nickel/manganese is 0.4.

2.2. X-ray diffraction

X-ray powder diffraction patterns have been recorded on a Phillips Xpert diffractometer using nickel-filtered Cu Kα (wavelength 0.154056 nm) radiation source and a scintillation counter detector. An aluminium holder was used to support the catalyst samples. The intensity data were collected over a 2θ range of 10–80° with a step size of 0.025° and a step time of 0.25 s. Crystalline phases were identified by comparison with the reference data from International Center for Diffraction Data (ICDD) files.

2.3. BET surface area and pore volume measurements

The BET surface area measurements were made by N_2 adsorption/desorption at liquid nitrogen temperature (77 K) using Micromeretics Gemini surface area apparatus. Prior to the analysis, 0.08–0.1 g of catalysts were evacuated under helium atmosphere for 2 h at 200 °C in the degassing port of the instrument. The adsorption isotherms of nitrogen were collected at 77 K using approximately six values or relative pressure ranging from 0.05 to 0.99 and by taking 0.162 nm^2 as the molecular area of the nitrogen molecule.

2.4. Temperature programmed reduction (H_2-TPR)

Hydrogen-TPR of various catalyst samples was performed using an automated catalyst characterization system (Micromeritics Model AutoChem 2910). Prior to the analysis approximately 50 mg of the catalysts were pre-treated at 200 °C for 2 h in ultra high pure helium (30 mL min^{-1}) stream after preheating, samples were tested by increasing the temperature from 50 to 800 °C. The temperature was then kept constant at 800 °C until the signal of hydrogen consumption returned to the initial values. The TPR runs were carried out with a linear heating rate (10 °C min^{-1}) in a flow of 4% H_2 in argon with a flow rate of 20 mL min^{-1}. The hydrogen consumption was measured quantitatively by a thermal conductivity detector. A mixture of isopropanol and liquid nitrogen was used in the trapper to collect the formed water during the TPR experiment.

2.5. In situ FT-IR spectroscopy

FT-IR spectra were recorded using a Bio-Rad (FTS-40). The scans were collected at a scan speed of 5 kHz, resolution of 2.0, and an aperture opening of 2.0 cm^{-1}. Sixteen scans were averaged for each normalized spectrum. Circular self-supporting thin wafers (8 mm diameter) consisting of 12 mg of material were used for the study. The wafers were placed in a high-temperature cell with CaF_2 windows and purged *in situ* in the IR cell with prepurified grade helium (30 mL min^{-1}, Wright Brothers) at 473 K for 2 h to remove any adsorbed impurities. After that, the samples were cooled to 323 K, and a background spectrum was collected before any gas adsorption. Afterward, NH_3 (3.9 vol% in He) was introduced to the cell with a flow of 30 mL min^{-1} for 1 h at 323 K to ensure complete saturation of the sample. Physisorbed ammonia was removed by flushing the wafer with helium for sufficient time (3 h) at 373 K. Subsequently, the FT-IR spectra were recorded by evacuation of ammonia at successive temperatures 323, 373, 423, 473, and 523 K.

2.6. X-ray photoelectron spectroscopy (XPS)

XPS was used to analyze the atomic surface concentration on each catalyst. The spectra were recorded on a Pyris-VG thermo scientific X-ray photoelectron spectrometer using Al Kα (1486.7 eV) as a radiation source at 300 W. The spectra were recorded in the fixed analyzer transmission mode with pass energies of 89.45 and 35.75 eV for recording survey and high resolution spectra, respectively. The powdered catalysts were mounted onto the sample holder and degassed overnight at room temperature at a pressure on the order of 10^{-7} Torr. Binding energies (BE) were measured for C 1s, O 1s, Ti 2p, Mn 2p, Cr 2p, Fe 2p, Co 2p, Ni 2p, Cu 2p, Zn 2p, Zr 3d, and Ce 3d. A recorded Auger spectrum for Mn was very weak. Sample charging effects were eliminated by correcting the observed spectra with the C 1s binding energy (BE) value of 284.6 eV [14]. An estimated error of 0.1 eV can be considered for all the measurements. The Mn 2p peak was deconvoluted using the Gaussian function, and a nonlinear background was subtracted.

2.7. Catalytic experiments

The catalytic activity measurement for the reduction of NO by ammonia (NH_3-SCR) with excess oxygen was carried out at atmospheric pressure in a fixed bed continuous flow quartz reactor with i.d. 6 mm. 0.1 g amount of catalyst (80–120 mesh) was placed in the reactor in between two glass wool plugs. The typical reactant gas composition was as follows: 400 ppm NO, 400 ppm NH_3, 2 vol% O_2 and He as balance. The premixed gases oxygen (4% in He, Wright Brothers), ammonia (3.99% in He, Wright Brothers), and nitric oxide (2.0% in He, Matheson) were used as received. The tubing of the reactor system was heat traced to prevent formation and deposi-

tion of ammonium nitrate. The NO and NO_2 concentrations were continually monitored by a chemiluminescence NO/NO_x detector (Eco Physics CLD 70S). To avoid modest errors caused by the oxidation of ammonia in the converter of the NO/NO_x analyzer, an ammonia trap containing phosphoric acid solution was installed before the sample inlet to the chemiluminescence detector [1]. The reactor was heated externally via a tubular furnace regulated by a temperature controller (Omega CN 2041), with a thermocouple inserted in to the catalyst bed. Prior to the catalytic experiments, the catalyst was activated *in situ* by passing oxygen (4% in He, Wright Brothers) for 2 h at 200 °C temperature. The reactants and products were analyzed *on-line* using a Quadrapole mass spectrometer (MKS PPT-RGA), chemiluminescence detector (Eco Physics CLD 70S) and a gas chromatograph equipped with TCD, and Porapack Q and Carboxen columns. Reactant and product contents in the reactor effluent were recorded only after steady state was achieved at each temperature step.

The NO conversions and N_2 selectivity were calculated as follows:

$$\text{NO conversion} \quad \% \quad (X_{NO}\%) = \frac{(C_{in} - C_{out})}{C_{in}} \times 100 \tag{1}$$

$$N_2 \quad \text{selectivity} = \left\{ \frac{N_2}{N_2 + N_2O + NO_2} \right\} \times 100 \tag{2}$$

In Eq. (1), C_{in} and C_{out} denoted the inlet and outlet gas concentrations of NO, respectively.

3. Results and discussion

3.1. X-ray diffraction

The powder X-ray diffraction patterns of various titania-supported manganese metal oxide, and co-doped manganese metal oxide samples calcined at 400 °C are shown in Fig. 1. The diffractogram patterns of pure TiO_2 anatase (Hombikat) are also presented for comparison. For pure TiO_2 sample, the strong characteristic peaks of titania typically at d = 3.54, 1.90, and 2.40 Å, which corresponds to anatase phase (JCPDS #71-1169) can be observed. Interestingly, our XRD studies of Mn/TiO_2 and $Mn–M'/TiO_2$ (M′ = Cr, Fe, Co, Ni, Cu, Zn, Ce, and Zr) samples revealed that the promoter oxides do not favour any titania phase transformation. For the Mn/TiO_2 catalyst with a manganese content 5 wt.% (M′/Mn = 0), X-ray reflections at d = 2.41, 1.63, and 2.11 Å (MnO_2 phase JCPDS #04-0779) are absent. This is a clear indication that manganese is in a highly dispersed state or the crystallites formed are less than 5 nm, and also insertion of manganese ions into the titania lattice [15]. For a series of $Mn–M'/TiO_2$ samples (with M′/Mn = 0.4), broad diffraction lines due to the titania anatase phase (JCPDS file #21-1272) could be observed in spite of high amount of titania anatase support. This would indicate that the co-doped metals (Cr, Fe, Co, Ni, Cu, Zn, Zr, Ce) and manganese oxides are highly dispersed on the titania support, and they are in amorphous or poorly crystalline state. This poor crystalline structure of manganese oxide has been suggested to improve the existence of oxygen vacancies and enhance catalytic performance [16].

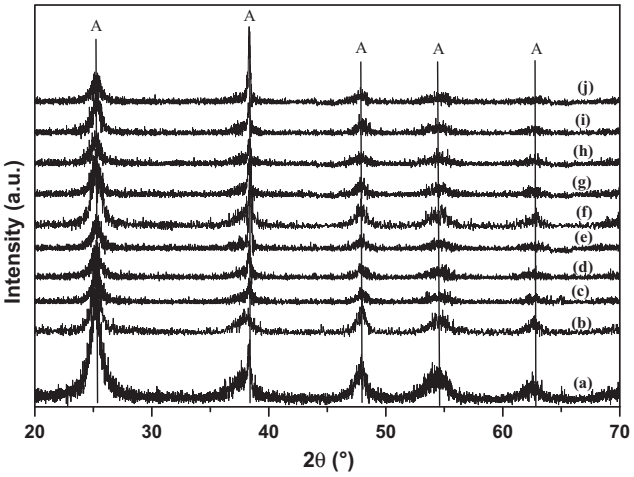

Fig. 1. Powder X-ray diffraction patterns of various titania-supported catalysts; (a) TiO_2 (Hombikat) (b) Mn/TiO_2 (c) $Mn–Cr/TiO_2$ (d) $Mn–Fe/TiO_2$ (e) $Mn–Co/TiO_2$ and (f) $Mn–Ni/TiO_2$ (g) $Mn–Cu/TiO_2$ (h) $Mn–Zn/TiO_2$ (i) $Mn–Zr/TiO_2$ (j) $Mn–Ce/TiO_2$, respectively.

3.2. BET surface area and pore volume measurements

The BET surface area, pore volume and pore size of the various catalysts are summarized in Table 1. The BET surface area of commercial TiO_2 anatase (Hombikat) sample obtained by N_2 physisorption at liquid nitrogen temperature was found to be 309 $m^2\ g^{-1}$. After the impregnation of manganese oxide onto the titania-support, the surface area dropped but the pore diameter increased greatly. However, the doping of a second metal to the Mn/TiO_2 is apparently enhanced the specific surface area of the particular $Mn–M'/TiO_2$ (M′ = Cr, Fe, Co, Cu, Zn, Ce, and Zr) catalyst. It can be seen that the surface area of the pure manganese oxide supported on titania is smaller than that of titania-supported bimetallic oxides catalysts (except $Mn–Zr/TiO_2$). An increase of the specific surface area by the substitution of other metal is in agreement with the literature [17]. Among the all the catalysts tested, $Mn–Ni/TiO_2$ catalyst attained the highest surface area (200 $m^2\ g^{-1}$) and the highest high pore volume (0.42 $cm^3\ g^{-1}$). The doping of sec-

Table 1
BET surface area and pore volume measurements of the prepared catalysts.

Catalyst	XRD phases	S_{BET} ($m^2\ g^{-1}$)	Average pore diameter (nm)	Pore volume ($cm^3\ g^{-1}$)	T (K)			
					T-1	T-2	T-3	T-4
TiO_2 Hombikat (commercial)	A	309	4.5	0.37	–	–	–	–
TiO_2 Hombikat[a]	A	161	9.3	0.42	–	–	–	–
$5Mn/TiO_2$	A	161	9.3	0.37	576	665	736	–
$5Mn–2Cr/TiO_2$	A	170	7.4	0.31	559	735	913	–
$5Mn–2Fe/TiO_2$	A	173	7.6	0.33	553	632	714	–
$5Mn–2Co/TiO_2$	A	160	8.4	0.33	519	708	739	–
$5Mn–2Ni/TiO_2$	A	200	8.6	0.42	510	684	–	–
$5Mn–2Cu/TiO_2$	A	166	8.6	0.35	402	475	670	–
$5Mn–2Zn/TiO_2$	A	179	6.7	0.29	523	622	706	865
$5Mn–2Zr/TiO_2$	A	150	7.9	0.29	545	627	738	894
$5Mn–2Ce/TiO_2$	A	167	7.7	0.32	525	628	741	880

Relative amounts are according to the metal wt.%; A – anatage;
[a] Calcined at 400 °C.

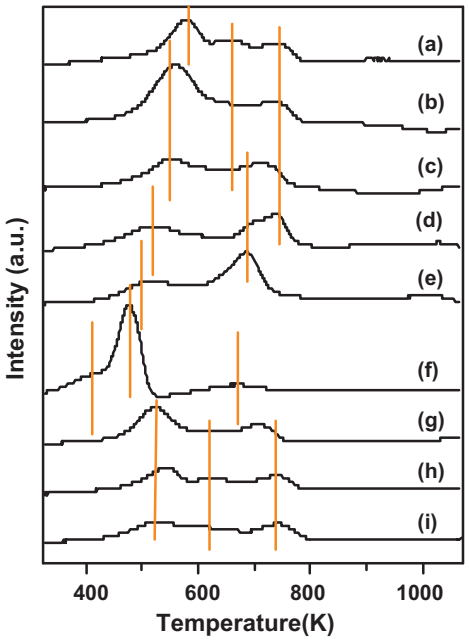

Fig. 2. (a) H_2-TPR patterns of (a) MnO_x/TiO_2 (b) Mn–Cr/TiO_2, (c) Mn–Fe/TiO_2, (d) Mn–Co/TiO_2, (e) Mn–Ni/TiO_2, (f) Mn–Cu/TiO_2, (g) Mn–Zn/TiO_2, (h) Mn–Zr/TiO_2, and (i) Mn–Ce/TiO_2; comparatively high shift of reduction peaks towards low-temperatures in MnO_x–Ni/TiO_2 catalysts.

ond metal can change the surface structure of the catalyst. It could be concluded that in the catalysts with the addition of a second metal, a lot of micropores could be conserved and the surface area is larger than that of the Mn/TiO_2. Among all the co-doped metals used, the specific surface area and pore volume of the Mn/TiO_2 catalyst are improved very much by doping the Mn/TiO_2 catalyst with nickel oxide.

3.3. Temperature programmed reduction (H_2-TPR)

For an adequate determination of effect of the second metal (M′) on the reduction profile of the Mn/TiO_2 catalyst, temperature programmed reduction (H_2-TPR) experiments were carried out in which the amount of manganese was kept constant (5 wt.%) and by regulating the second metal of the catalyst. The corresponding TPR profiles are presented in Fig. 2. Three different reduction peaks are observed for the pure Mn/TiO_2 catalyst. The low-temperature reduction peaks at 576 K (T_1), 665 K (T_2), and 736 K (T_3) can be interpreted as a stepwise reduction of MnO_2 to Mn_2O_3, Mn_2O_3 to Mn_3O_4 and Mn_3O_4 to MnO, respectively (Table 1). The Mn/TiO_2 catalyst does not contribute much to the partial reduction of titania support (Ti^{4+} to Ti_4O_7).

The reduction temperatures of all the titania-supported mixed oxides are significantly decreased when compared to the pure individual promoter oxides. The reduction profiles of bulk CrO_3 consist of reduction peaks at 553, 735, and 858 K. The hydrogen reduction of Cr^{6+} to Cr^{5+} Cr^{5+} to Cr^{3+} and Cr^{3+} to either Cr^{2+} or to the metallic state occurs at about 553, 735, 858 K, respectively [18]. The reduction profile peaks of our Mn–Cr/TiO_2 catalyst appeared at 559, 735, and 913. The peak at 559 K could be due to the reduction of both chromium and manganese species and later are for the reduction of Cr^{5+} to Cr^{3+} and Cr^{3+} to either Cr^{2+} or to Cr^0. It is suggested that Cr reduction is dominant over the manganese species in the Mn–Cr/TiO_2 catalyst, which may be due to the coverage of manganese species by the chromium ions. However, H_2-consumption peaks of manganese species are shifted to lower temperatures by the addition of Cr_2O_3 to Mn/TiO_2 catalyst.

A low temperature reduction peak (T_1) is observed at 576 K in Mn/TiO_2 catalyst. After substitution of the iron (Fe_2O_3) species, this (manganese reduction) peak is shifted to 553 K. In our previous study, we have concluded that the reduction of iron species in Fe_2O_3/TiO_2 shows a reduction peak at 660 K [19], this (iron reduction) peak is shifted to 632 K in Mn–Fe/TiO_2 catalyst. On the other hand, Mn–Co/TiO_2 catalyst shows three distinct peaks at 519, 708, and 739 K. The low temperature peak at 519 K is corresponding to the reduction of manganese species. The later peaks at 708, 739 K are attributed to the Co^{3+} to Co^{2+} and Co^{2+} to Co^0 transitions, respectively [20,21].

Subsequently, the addition of NiO to the Mn/TiO_2 showed two distinct peaks at 510 and 684 K. The low temperature reduction peak (T_1) of manganese species is significantly shifted from 576 K to 510 K. Among all the catalysts (except copper promoted), Mn–Ni/TiO_2 showed the highest shift of the manganese reduction temperature and could be an indication of positive interaction between the titania support and the manganese–nickel oxide species [22,23]. This interaction may be an enhancement of the oxygen mobility. It means the oxygen mobility was greatly enhanced due to the introduction of nickel oxide, which was beneficial to the SCR reaction. The hydrogen consumption peak at 684 K is attributed to the transition of Ni^{2+} to Ni^0 [19].

The comparison with the H_2-consumption curves obtained over the corresponding single-oxide and in the mixed-oxide catalyst shows that manganese oxides contained in the Mn–Ni/TiO_2 sample are reduced at much lower temperatures in the presence of nickel oxide. The absence of the high-temperature (736 K) peak indicates that the dominant phase is MnO_2. Thus, mixing manganese and nickel oxides results in stabilization of the former oxide in the form of MnO_2, which is reduced at lower temperatures, compared to Mn_2O_3 [16]. This increase of reducibility and dominant phase of MnO_2 seems to be the reason for the increased activity of Mn–Ni/TiO_2 catalysts, compared to the corresponding single oxide and other mixed oxide catalysts.

The reduction profile of Cu/TiO_2 is characterized by two reduction peaks at 450 and 485 K [24]. In the present study, three different peaks are observed in the TPR profile of the Mn–Cu/TiO_2 catalyst at 402, 475, and 670 K. The broad reduction peak centered at 402 K can be attributed to the reduction of CuO particles being in strong interaction with the titania support. The sharp reduction peak centered at 475 K can be ascribed mainly to the reduction of CuO particles having little or no interaction with the support. This assignment appears to be in agreement with literature data [24]. A broad peak at 670 K can be due to the reduction of manganese species. The reduction of ZnO particles is difficult under TPR environment has been demonstrated earlier [25]. The reduction profile of Mn–Zn/TiO_2 exhibited very slight H_2 consumption at 865 K and can be ascribed to an insignificant reduction of surface zinc oxide. This occurrence and catalytic activity of Mn–Zn/TiO_2, both suggest that zinc oxide is not promoting the Mn/TiO_2 catalyst.

Mn–Zr/TiO_2 reduction profile shows three sharp peaks at 545, 627, and 738 K, all of these peaks correspond to the reduction of the surface manganese oxide reduction. One broad peak was also observed at 894 K. It is known that zirconium oxide has two different surface hydroxyl groups (bridged and terminal). We ascribe the characteristic broad TPR peak at 894 K to the reductions of these two hydroxyl groups [26]. Addition of zirconia does not create any variation in the reduction pattern of Mn/TiO_2 catalyst. There are only marginal changes in T_{max} positions of manganese species in Mn–Zr/TiO_2 catalyst for the studied temperature range. The TPR patterns of Mn–Ce/TiO_2 catalyst showed four peaks at 525, 628, 741 and 880 K owing to the surface manganese oxide species reduction. The peak at 628 K is probably associated also with reduction of the surface oxygen of ceria [27,28]. The peak at 880 K is likely due to the formation of nonstoichiometric cerium oxides [29]. The

Table 2
Binding energy, surface atomic ratio of M′/Mn, Mn/Ti, and Mn^{4+}/Mn^{3+} for Mn–M′/TiO_2 catalysts determined from deconvoluted XPS spectra.

Catalyst	B.E. (eV)					M′		(Mn^{4+}/Mn^{3+})[a]	M′/Mn[a]	Mn/Ti[a]
	Ti $2p_{3/2}$	Ti $2p_{1/2}$	O 1s	Mn $2p_{3/2}$	Mn $2p_{1/2}$					
5Mn/TiO_2	458.6	464.3	529.9	642.1	653.6	–	–	02.02	–	0.13
				641.3	653.0					
5Mn–2Cr/TiO_2	458.6	464.4	530.2	642.1	653.6	$2p_{3/2}$	$2p_{1/2}$	02.20	1.57	0.10
				641.3	653.0	578.7	587.7			
5Mn–2Fe/TiO_2	458.9	464.4	530.5	642.1	653.6	$2p_{3/2}$	$2p_{1/2}$	12.67	0.39	0.11
				641.3	653.0	711.9	725.0			
5Mn–2Co/TiO_2	458.5	464.2	529.9	642.1	653.6	$2p_{3/2}$	$2p_{1/2}$	03.43	0.75	0.09
				641.3	653.0	780.9	797.7			
5Mn–2Ni/TiO_2	459.1	464.6	530.3	642.1	653.6	$2p_{3/2}$	$2p_{1/2}$	22.31	0.43	0.13
				641.3	653.0	856.3	874.6			
5Mn–2Cu/TiO_2	458.6	464.1	530.0	642.1	653.6	$2p_{3/2}$	$2p_{1/2}$	07.91	0.83	0.05
				641.3	653.0	934.0	953.7			
5Mn–1Zn/TiO_2	458.7	464.2	530.2	642.1	653.6	$2p_{3/2}$	$2p_{1/2}$	02.55	0.79	0.06
				641.3	653.0	1021.8	1044.6			
5Mn–3Zr/TiO_2	458.8	464.3	530.2	642.1	653.6	$3d_{3/2}$	$3d_{5/2}$	01.34	0.61	0.10
				641.3	653.0	182.2	184.6			
5Mn–2Ce/TiO_2	458.6	464.3	530.1	642.1	653.6	$3d_{3/2}$	$3d_{5/2}$	03.05	0.34	0.11
				641.3	653.0	884.3	901.9			

M′ – co-doped metal.
[a] Relative amounts are according to the metal atomic ratio.

titania-supported manganese catalyst does not contribute much to the reduction of Ti^{4+} to Ti_4O_7, but in the case of Mn–M′/TiO_2 catalysts, one peak appeared at around 1000 K. This peak corresponds to the partial reduction of titania support. This is a clear indication to suggest that the substitution of second metal is promoting the catalyst for the partial reduction of TiO_2 to Ti_4O_7. An average intensity peaks are observed at 865, 894 and 880 K for the Mn–Zn/TiO_2, Mn–Zr/TiO_2 and Mn–Ce/TiO_2 catalysts, respectively (Fig. 2, Table 2). Which are due to the partial reduction of titania support (Ti^{4+} to Ti_4O_7). Due to the differentiation in the intensity ratio, corresponding peaks are not evident when we put all the graphs together. This is the reason why the features above 800 K are not evident in Fig. 2 spectra. One can observe a clear peak at 880 K in the Mn–Ce/TiO_2, at 865 K in Mn–Zn/TiO_2 and at 894 K in Mn–Zr/TiO_2 in their individual H_2-TPR spectra.

3.4. Adsorption of ammonia – FT-IR spectroscopy

The adsorption and desorption characteristics of NH_3 over the Mn/TiO_2 and Mn–M′/TiO_2 (M′ = Cr, Fe, Co, Cu, Zn, Ce, and Zr) catalysts have been extensively investigated to ensure the effect of co-doping metal. A number of *in situ*-FTIR experiments were performed to gain a better understanding of molecular behaviour of ammonia and to acquire the information about surface species of the low-temperature SCR catalysts. The adsorption–desorption of ammonia provided information about the nature of acid sites present, and its presence as a function of temperature (323–523 K) revealed the potential strength of the acid sites.

In line with results reported previously, the spectra of ammonia adsorbed on TiO_2 anatase after evacuation at various temperatures shows only bands assigned to ammonia coordinatively adsorbed on Lewis sites [30,31]. In the higher frequency region, multiplicity of the bands makes it difficult to identify the particular acidic sites [31]. The bands in the NH stretching region (via a Fermi resonance interaction) split in part, and give rise to bands at 3142, 3190, 3230, 3259, 3294, 3352, and 3387 cm^{-1} (not shown). When only Mn is added to the support, an important phenomenon occurs. The 1167, 1301, 1467, 1599, and 1680 cm^{-1} peaks are observed for Mn/TiO_2, all these peaks are corresponding to ammonia coordinatively adsorbed on Lewis sites.

The *in situ*-FTIR spectra of ammonia adsorbed over the Mn–Cr/TiO_2 catalyst followed by evacuation at successive temperatures are presented in Fig. 3a. Evidently, in addition to the bands near 1601 and 1171 cm^{-1} (δ_{as} NH_3, δ_s NH_3 bound to Lewis acid sites, respectively) a broad absorption band at 1438 cm^{-1} due to δ_{as} NH_4^+ vibrations with a shoulder near 1480 cm^{-1} and another band at 1678 cm^{-1} ascribed to δ_s NH_4^+ are also detected. Interestingly, evacuation at above 423 K causes the disappearance of these δ_{as} NH_4^+, δ_s NH_4^+ absorptions.

The spectra recorded after adsorption of ammonia over the Mn–Fe/TiO_2 followed by outgassing at various temperatures (Fig. 3b) are characterized by a strong broad band at 1128–1284 cm^{-1} with a maximum at 1164 cm^{-1} and an evident shoulder component near 1223 cm^{-1}. The 1128–1284 cm^{-1} band is attributed to δ_s NH_3 coordinated to Lewis acid sites [32]. In addition, two strong bands centered at 1552 and 1604 cm^{-1} observed are ascribed to δ_{as} NH_3 coordinated to Lewis acid sites [33,34]. Finally, three weak peaks are found at 1304, 1360 and 1432 cm^{-1}. The peak at 1304 cm^{-1} due to the δ_s NH_3 vibrations which are coordinated to Lewis acid site, whereas later peaks are assigned to asymmetric and symmetric deformations of ammonium ion, respectively. Evacuation at increasing temperatures originates a relevant sharpening of the band. Although the catalytic reduction of NO results demonstrated that the Mn–Fe/TiO_2 is improved than the Mn/TiO_2 catalyst, the *in situ* NH_3-FTIR spectra illustrated the Mn–Fe/TiO_2 catalyst is a medium strength Lewis acid solid.

In situ contact of ammonia with Mn–Co/TiO_2 catalyst at 323 K and followed by degassing at different temperatures cause the formation of sharp and strong bands at 1158, 1212, 1544 and 1596 cm^{-1} and also weak bands at 1290, 1344, 1426 cm^{-1} (Fig. 3c). Extremely strong peaks with a maximum at 1158, 1212 cm^{-1} are ascribed to δ_s NH_3 bound to Lewis acid site. Strong bands at 1544 cm^{-1} and 1596 cm^{-1} are intended for δ_{as} NH_3 bound to Lewis acid sites. Low intense bands at 1290, 1344, 1426 cm^{-1} are assigned to the δ_{as} NH_4^+ vibrations.

The *in situ*-FTIR spectra of ammonia adsorbed over the Mn–Ni/TiO_2 catalyst followed by evacuation at successively increasing temperatures are presented in Fig. 3d. We observed similar characteristic spectra as Mn/TiO_2. In both cases the features of coordinative adsorbed species (1098, 1156 and 1228 cm^{-1}, δ_s NH_3 bound to Lewis acid sites) are observed. These results suggest that the manganese (Mn/TiO_2) and manganese–nickel (Mn–Ni/TiO_2) surface sites are having Lewis acidity, with no apparent Brönsted acidity. Interestingly, an absorption peak at 1156 cm^{-1} (δ_s NH_3 coordinated to Lewis acid sites) decrease down to disappear after evacuation at 473–523 K range. Bands at 1540 and 1599 cm^{-1} are

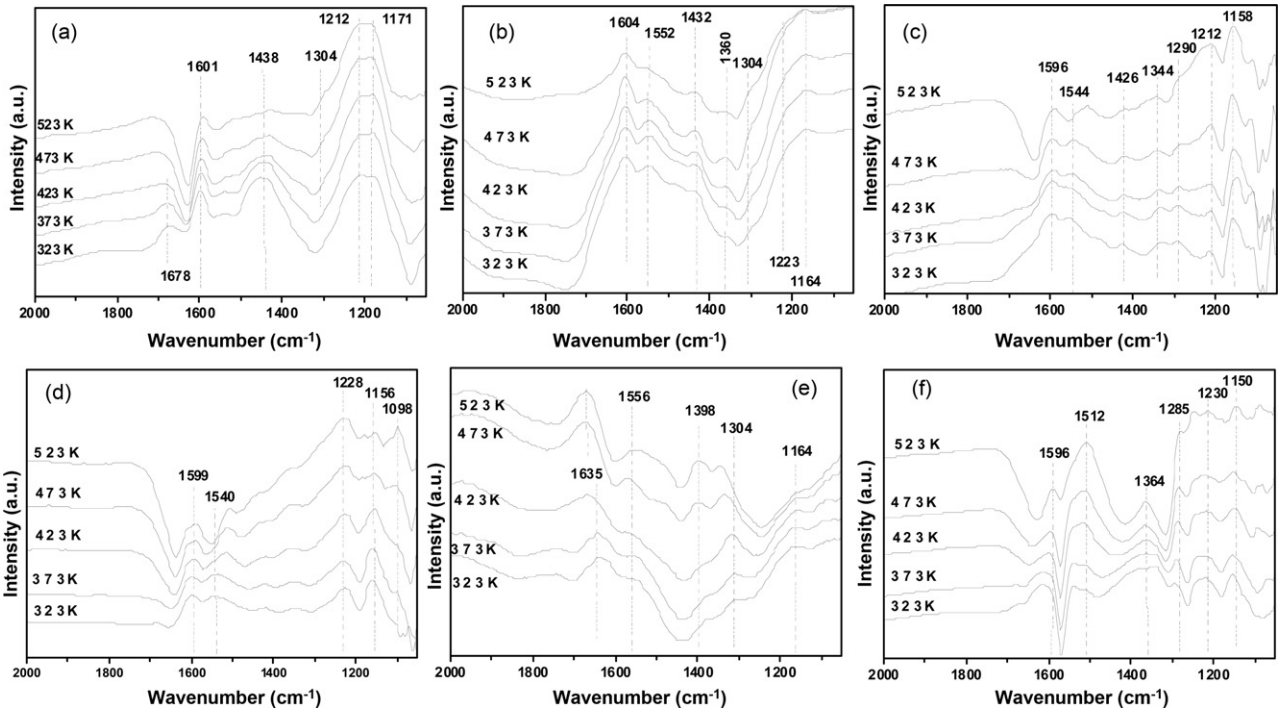

Fig. 3. *In situ* FT-IR spectra of coordinatively held ammonia species, adsorbed at 323 K over the Mn–M′/TiO_2 catalysts and successively increasing temperatures up to 523 K, while evacuating; (a) Mn–Cr/TiO_2 (b) Mn–Fe/TiO_2, (c) Mn–Co/TiO_2, (d) Mn–Ni/TiO_2, (e) Mn–Cu/TiO_2, and (f) Mn–Zn/TiO_2.

attributed to the δ_{as} NH_3 coordinated to Lewis acid sites. Red shift in 1540 cm^{-1} band is observed, which could be due to the weakening of M^{n+}–NH_3 bond.

When ammonia was adsorbed at 323 K over the Mn–Cu/TiO_2 catalyst, different bands were observed while evacuation at the temperatures range 323–523 K (Fig. 3e). The four strong bands at 1164, 1304, 1556, and 1635 cm^{-1} are assigned to ammonia vibrations on Lewis-acid sites. The absorption peaks at 1304, 1398 cm^{-1} are being possibly associated to a species intermediate with respect to the formation of other species. Intensity of the peaks at 1304 cm^{-1} and 1398 cm^{-1} was very low at low temperatures and increased after 373 K. These features suggest that ammonia is decomposed by heating before desorption, and indicate that the reaction of ammonia can occur over the surface of copper oxide [34]. The band at 1635 cm^{-1} which is due to asymmetric deformation of coordinated NH_3 is blue shifted at high temperatures (473–523 K) [34]. Evacuation at increasing temperatures caused the intensity of the 1164 cm^{-1} peak to decrease and eventually disappear.

The *in situ*-FTIR spectra of the adsorbed ammonia over the surface of Mn–Zn/TiO_2 catalyst followed by evacuation with respect to the reaction temperatures are shown in Fig. 3f. An extremely strong band at 1512 cm^{-1} is assigned to an amide species scissoring mode [35]. An additional strong band at 1364 cm^{-1} is assigned to ammonium ions [36]. Thus, ammonia is thought to undergo both protonation to ammonium ion and deprotonation to amide anion. This disproportionation progression is due to the direct proton exchange in ammonia. Intensity of the band at 1512 cm^{-1} increased at high temperatures. On the other hand, Intensity of the bands at 1150, 1230, 1285, 1596 cm^{-1} decreased at high temperatures suggesting that weak Lewis acidic sites are present in the Mn–Zn/TiO_2. The splitting of the symmetric deformation mode at 1230 cm^{-1}, most sensitive to the acidic strength of the surface sites, shows that two different adsorbing centers are active.

The FTIR spectra of the adsorbed species arising from the interaction of ammonia with the surface of Mn–Zr/TiO_2 and evacuation at various temperatures are very complex and reflect the complex chemistry of ammonia-catalyst (not shown). Ammonia adsorbed species on the titania-supported manganese–cerium oxide were investigated by *in situ*-FTIR spectroscopy (not shown). Several peaks at 1123, 1156, 1209, 1334, 1460, 1517, and a weak peak at 1620 cm^{-1} could be observed. The bands at 1123, 1156, 1209, and 1620 cm^{-1} peaks were attributed to coordinatively adsorbed NH_3 on Lewis sites. While, the band at 1517 cm^{-1} was assigned to an amide species scissoring mode, formed by hydrogen abstraction from coordinated ammonia [37,38]. The band at 1460 cm^{-1} is attributed to the δ_{as} NH_4^+ vibrations of ammonium ions bound to Brönsted acid sites [38]. However, these bands are disappeared at high temperatures suggesting that with the addition of ceria, very weak Brønsted acid sites are formed over the surface of Mn/TiO_2 catalyst.

3.5. X-ray photoelectron spectroscopy

For the reference manganese phase compounds, commercial samples of MnO_2, Mn_3O_4, and MnO (Sigma–Aldrich) were used. In addition MnO_2 and Mn_2O_3 were prepared using aqueous solutions of manganese nitrates [39], Mn_3O_4 was prepared by the slow reduction of MnO_2 at 473 K in H_2 [40]. Titania anatase supported manganese and co-doped manganese catalysts were investigated by X-ray photoelectron spectroscopy to identify the chemical compositions (atomic concentrations) of the surface layer and to ensure the oxidation states of manganese oxides, and co-doped metal interacting with titania support on each catalyst (Table 2). For all the prepared samples, two main peaks due to Mn $2p_{3/2}$ and Mn $2p_{1/2}$ were observed from 639 eV to 658 eV. It has been established in the literature and found in our studies that the $2p_{3/2}$ binding energy of metallic Mn (Mn^0) and MnO_2 (Mn^{4+}) was 639.0 eV and 642.1 eV, respectively [5,41,42]. Hence, it is highly difficult to distinguish the oxidation states of manganese species without peak deconvolution since there is only less than 1 eV binding energy difference between each manganese phase. To better understand the surface

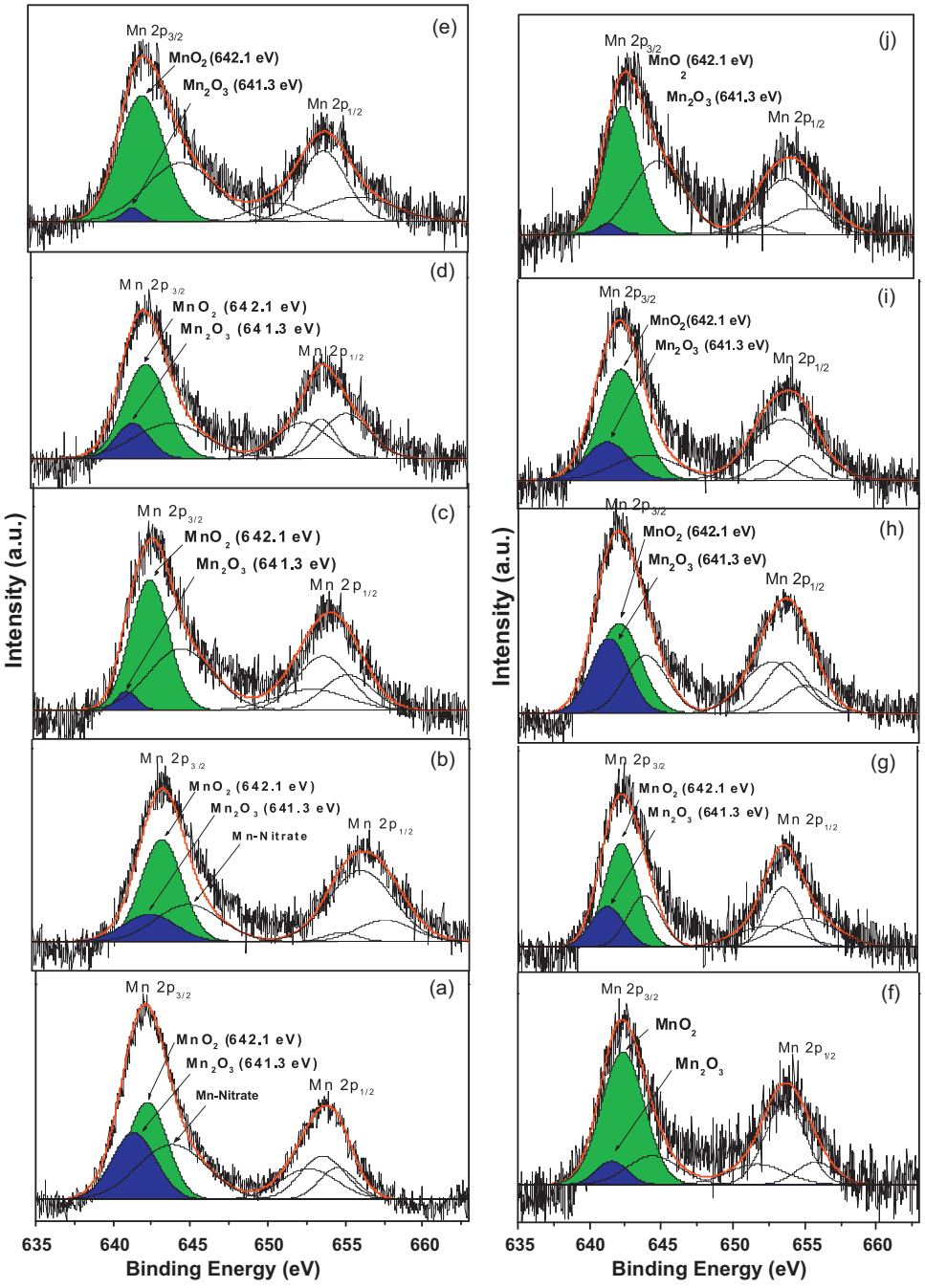

Fig. 4. Deconvoluted Mn 2p (XPS) spectra of (a) MnO_x/TiO_2 (b) Mn–Cr/TiO_2, (c) Mn–Fe/TiO_2, (d) Mn–Co/TiO_2, (e) Mn–Ni/TiO_2, (f) Mn–Cu/TiO_2, (g) Mn–Zn/TiO_2, (h) Mn–Zr/TiO_2, (i) Mn–Ce/TiO_2, and (j) spent Mn–Ni/TiO_2 catalysts.

manganese oxide phases and their relative intensities, the overlapped Mn 2p peaks were deconvoluted into several sub-bands by searching for the optimal combination of Gaussian bands with the correlation coefficients (r^2) above 0.99 (PeakFit, Version 4.0.6, AISN Software Inc.) without fixing the sub-band positions. The deconvoluted peaks are signed as specific phases of manganese in each spectrum (Fig. 4).

All binding energy data presented in Table 2 have been adjusted against the C ls peak standardized at 284.6 eV [43]. With Al Kα radiation, the Mn 2p peaks for pure manganese phases were also recorded to evaluate the specific surface manganese oxide phases and correlated with our catalysts to find out Mn^{4+}/Mn^{3+} ratio (Table 2). Two main peaks of pure MnO_2 (Mn^{4+}) sample due to Mn $2p_{3/2}$ and Mn $2p_{1/2}$ were observed at 642.1–653.6 eV, respectively. In case of pure Mn_2O_3 (Mn^{3+}) sample, Mn $2p_{3/2}$ and Mn $2p_{1/2}$ were pragmatic at 641.3–653.0 eV, respectively. Consequently, the $2p_{3/2}$ binding energies at 642.1 and 641.3 eV are attributed to the presence of surface Mn^{4+} and Mn^{3+} species in the catalyst.

SCR of NO over the pure manganese oxides at low-temperature was investigated by Kapteijn et al. [13] and found that the NO conversions decreased in the order of $MnO_2 > Mn_5O_8 > Mn_2O_3 > Mn_3O_4$. In a similar manner, in our present work it is worth noting that the MnO_2 phase is extremely dominant over the Mn_2O_3 phase in nickel-codoped titania-supported manganese catalysts (Mn^{4+}/Mn^{3+} = 22.31, 96%), whereas Mn_2O_3 phase is in competition with MnO_2 in other catalysts (Mn^{4+}/Mn^{3+} = 1.34–12.67) (Fig. 4). These results are in good accordance with the H_2-TPR measurements, whereas only two peaks

($MnO_2 \rightarrow Mn_2O_3$ and $NiO \rightarrow Ni$) were observed for the Mn–Ni/TiO_2 sample. Comparing to other metals co-doped Mn oxides supported on TiO_2 catalysts; it is evident that the Mn/Ti atomic ratio of Mn–Ni/TiO_2 is significantly high in contrast to other optimized catalysts. This is due to the higher surface coverage by manganese oxide and/or its higher dispersion on the TiO_2 support.

In addition, high surface concentrations (M′/Mn) of co-doped metals such as, Cr^{3+} (Cr_2O_3), Cu^{2+} (CuO), Zn^{2+} (ZnO), Co^{3+}, Co^{2+} (Co_3O_4), and Zr^{4+} (ZrO_2) are observed for the corresponding catalysts (Table 2). In the same manner, very low concentration of surface manganese species (Mn/Ti) is observed for the same catalysts. Accordingly, it can be suggested that the surface manganese species are predominantly covered by the co-doping metal oxide species in these Mn–M′/TiO_2 (M′ = Cr, Cu, Zn, Co, Zr) catalysts. This is one of the reasons for the low activity of these catalysts. On the other hand, rational low concentrations of co-doped metal are observed for the Mn–Ce/TiO_2 (Ce_2O_3), Mn–Fe/TiO_2 (Fe_2O_3), and Mn–Ni/TiO_2 (NiO) catalysts. It can be suggested from both the suggested from the both M′/Mn, and Mn/Ti values, only Mn–Ni(0.4)/TiO_2 catalyst exhibits a high concentration and coverage of surface manganese and a low concentration of highly dispersed co-doped metal.

3.6. Catalytic performance of Mn/TiO_2 and co-doped MnO_x/TiO_2 catalysts

In each experiment, five samples of (M′) co-doped MnO_x/TiO_2 catalysts were used to study the effect of co-cations loading as a function of M′/Mn atomic ratio with respect to the temperature (160–240 °C) in the SCR of NO by ammonia. Each sample had a constant loading of manganese and different loading of second metal. Prior to the catalytic performance tests, a reaction with Hombikat TiO_2 catalyst (calcined at 400 °C) was performed at 250 °C to observe the catalytic activity of the TiO_2 support and the efficiency of SCR unit. As expected, the NO and NH_3 conversions were zero when only TiO_2 anatase (Hombikat) was used as catalyst at relevant conditions (not shown in figure). Pure MnO_x/TiO_2 shows 70% NO conversion at 200 °C.

Initially, we evaluated the potential catalytic performance of the prepared Mn–Cr/TiO_2 (Cr/Mn atomic ratio = 0, 0.2, 0.4, 0.6, 0.8) catalysts to optimize the Cr content and to ensure the influence of Cr^{n+} co-cations on NO conversion with respect to the temperature (160–240 °C). The catalytic performance results for the SCR of NO with ammonia over titania-supported manganese as well as manganese–chromium catalysts are tested at GHSV 50,000 h^{-1} in the presence of 2 vol% of oxygen (Fig. 5a). From our results we can observe that, the substitution of partial Mn with chromium elements could indeed influence the SCR activity of Mn/TiO_2 catalyst. Under identical operating conditions, among all the Mn–Cr/TiO_2 (Cr/Mn = 0, 0.2, 0.4, 0.6, 0.8) catalysts tested the Mn–Cr/TiO_2 catalysts with Cr/Mn atomic ratio = 0.2, 0.4 have demonstrated a good performance giving 88 and 90% conversions, respectively at 180 °C. However, at temperatures higher than that, the NO conversions decreased rapidly to the 23% (Mn–Cr(0.2)/TiO_2), and (Mn–Cr(0.4)/TiO_2). In comparison with Mn/TiO_2, the NO conversions increased with the Cr/Mn ratio equal to 0.2, 0.4 and then decreased for higher loadings of chromium (Cr/Mn = 0.6 and 0.8). This is due to the existence of the bulk amount of chromium oxide in the sample which can block the manganese active pores present over the surface of catalyst. These results suggest that the optimal content of chromium is reached with the Cr/Mn atomic ratio equal to 0.4 at optimal temperature 180 °C for maximum NO conversion.

Fig. 5b shows the NO conversion as a function of Fe content with respect to the temperature range (160–240 °C) in the NH_3-SCR reaction over Mn–Fe/TiO_2 catalysts. From these results, we can observe the influence of Fe^{n+} co-cations on the SCR activity of Mn/TiO_2 catalyst. Near at 200 °C the substitution of the Fe content to Mn (Fe/Mn) equal to 0.4 could obviously enhance the NO conversions (87%), while the NO conversions drop off to a certain extent at higher temperatures. Pure Mn/TiO_2 and Mn–Fe/TiO_2 showed very narrow operation temperature windows in the low temperature ranges. Both of the maximum NO conversions could not reach 100% but the NH_3-SCR activity and stability of the Mn/TiO_2 catalyst improved greatly by the addition of optimal iron content (Fe/Mn atomic ratio = 0.4) for high NO conversion.

NH_3-SCR performances of various cobalt co-doped Mn/TiO_2 catalysts were measured as a function of temperature and the Co/Mn ratio based on atomic percentage (Fig. 5c). For the catalyst with 0.2 Co/Mn atomic ratio, NO conversion (62%) starts at 160 °C and reaches 78% at 200 °C. The onset NO conversion of NH_3-SCR reaction at 200 °C, decreases down to 57%, 53% for the catalysts having Co/Mn ratio 0.6 and 0.8, respectively. For those catalysts with higher cobalt content, NO conversions were dropped to 40% (Co/Mn = 0.6) and 37% (Co/Mn = 0.8) at about 240 °C. Thus, the ratio of Co/Mn plays an important role in promotion of Mn/TiO_2 catalyst for the low-temperature NH_3-SCR reaction. Among these Mn–Co(x)/TiO_2 (x = 0, 0.2, 0.4, 0.6, 0.8) catalysts, with Co/Mn ratio 0.2 and 0.4 showed good low-temperature NH_3-SCR activity. Eventually, the addition of cobalt improved the SCR performance of the Mn/TiO_2 catalyst but could not broaden the temperature window and could not reach to 100% NO conversions.

On the other hand, the nickel loading has a strong influence on the conversion, since nickel loading with the Ni/Mn ratio = 0.4 catalyst exhibits a maximum conversion of 100% at 200 °C (Fig. 5d). This would indicate that an optimal dispersion of Mn–Ni species on the support surface is attained with this amount of nickel in the Mn–Ni/TiO_2 catalyst to reach the high NO conversion. Moreover, from BET surface area analysis, it was determined that only nickel co-cations show the highest surface area and pore volume thus, in consequence, enhanced SCR activity. The addition of nickel species to the Mn/TiO_2 catalyst (Ni/Mn ratio = 0.4) broaden the temperature window and shows 100% NO conversion at the temperature range 200–250 °C. Doping of nickel co-cations greatly improved the thermal stability of the Mn/TiO_2 catalyst, Mn–Ni(0.4)/TiO_2 catalyst showed 76% NO conversion even at 300 °C (not shown). This result was expected since the H_2-TPR curve for the 5Mn–2Ni/TiO_2 catalyst showed the highest shift in reduction peaks towards lower temperatures.

Further increase in the nickel content exceeding than 0.4 Ni/Mn atomic ratio, decreased the SCR activity of catalyst to 81% and 77% (for the ratio 0.6, 0.8 catalysts, respectively) at optimal temperature 200 °C. This is due to the interaction between the TiO_2 and manganese–nickel oxide becomes weak and the number of participating surface manganese oxide sites decrease with the raise of nickel loading. All the above results showed that nickel is effectively promoting the NH_3-SCR activity at low-temperatures and broadening the temperature window (thermal stability) performance of titania-supported manganese catalyst. Therefore, it has concluded that the nickel oxide had interacted with manganese oxide and titania as a result, preventing the sintering, and then higher catalytic activity was obtained.

The co-doping of copper in titania-supported manganese catalysts could enhance the SCR activity. To observe the influence of copper co-cations and the effect of their atomic ratio with manganese, various Mn–Cu/TiO_2 catalysts with the function of Cu/Mn ratio = 0, 0.2, 0.4, 0.6, 0.8 are tested at the temperature range 160–240 °C (Fig. 5e). The NH_3-SCR activity of the Mn–Cu/TiO_2 catalysts with 0.4 and 0.2 Cu/Mn ratios had an obvious increase owing to the optimal high dispersion of copper–manganese oxides on titania support, especially at optimal 200 °C. The SCR activity and broadening of temperature window at the temper-

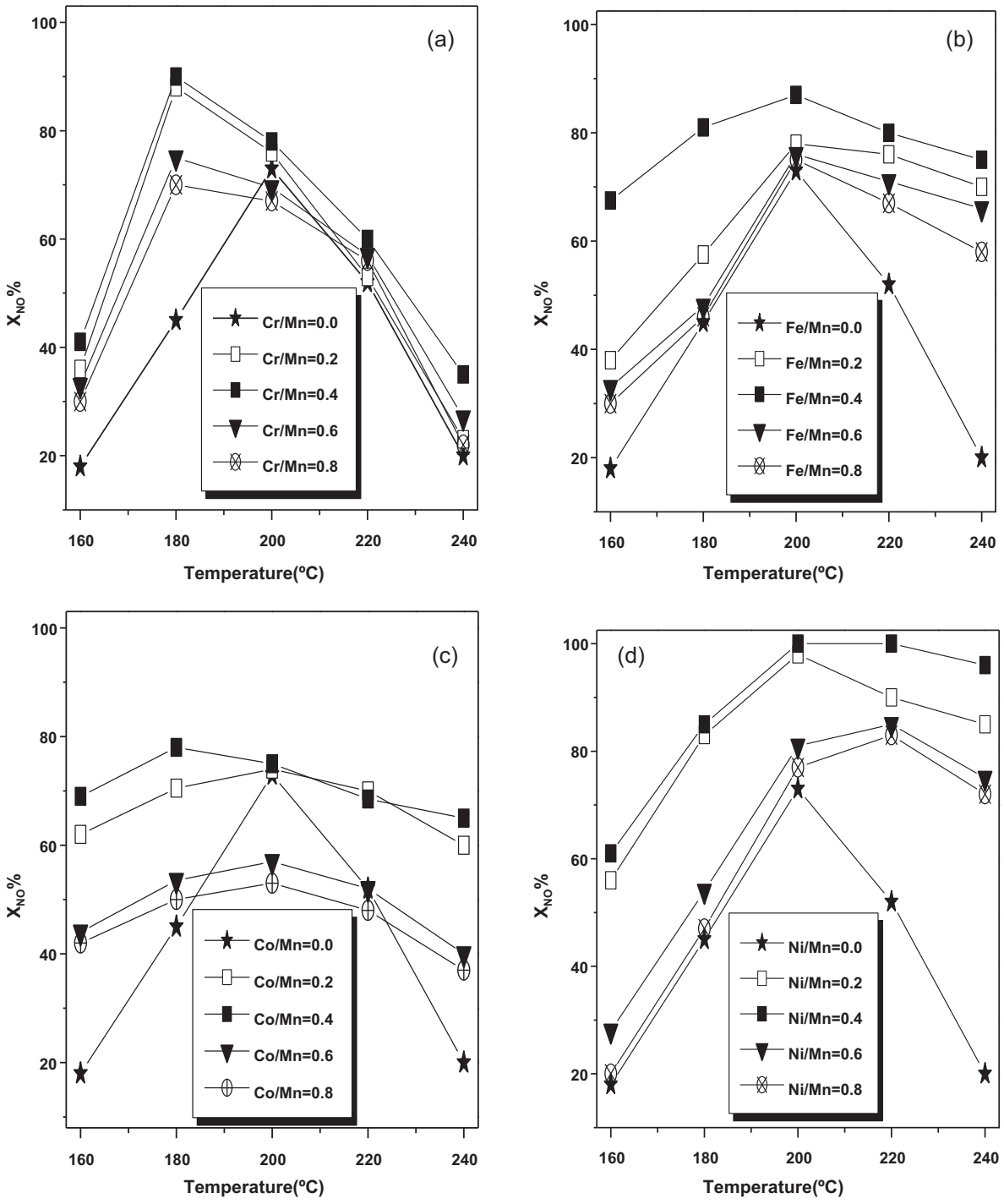

Fig. 5. Influence of M′/Mn atomic ratio on NO conversion in the SCR reaction at a temperature range (160–240 °C) over Mn–M′/TiO_2 catalysts; GHSV = 50,000 h^{-1}; feed: NO = 400 ppm, NH_3 = 400 ppm, O_2 = 2 vol%, He carrier gas, catalyst = 0.1 g, total flow = 140 mL min^{-1}. X_{NO}% = conversion of NO at 6 h on stream.

ature range 160–240 °C decreased in the following sequence: Mn–Cu(0.4)/TiO_2 > Mn–Cu(0.2)/TiO_2 ≅ Mn–Cu(0.6)/TiO_2 > Mn–Cu(0.8)/TiO_2 ≫ Mn–Cu(0)/TiO_2.

NO reduction by NH_3 in the presence of excess oxygen was carried out over zinc co-doped Mn/TiO_2 catalysts at low-temperatures. Fig. 5f shows the NO conversion as a function of temperature over various Mn–Zn/TiO_2 catalysts based on Zn/Mn atomic ratio during the NH_3-SCR reaction. Unlike the other promoters zinc cations had a different optimal ratio with manganese to achieve the high NO conversion in the SCR reaction. Among the all zinc doped Mn/TiO_2 catalysts, Mn–Zn/TiO_2 catalyst with Zn/Mn = 0.2 showed improved activity. By increasing the loading of zinc oxide (Zn/Mn = 0.4, 0.6, 0.8) over the surface of titania, SCR activity dropped to lower than Mn/TiO_2 catalyst. Since that the amount of surface zinc oxide is low and manganese oxide sites are active for the initial case, these the manganese oxide pores may be blocked by increasing of the amount of zinc oxide over the titania support in the later catalysts. These results are in agreement with literature, where the addition of too much (a saturation point of 1.5 wt.%) zinc leads to a decrease in SCR activity of the catalyst [44,45].

In order to compare the influence of co-cations and activities of titania supported various bimetallic oxides, different cata-

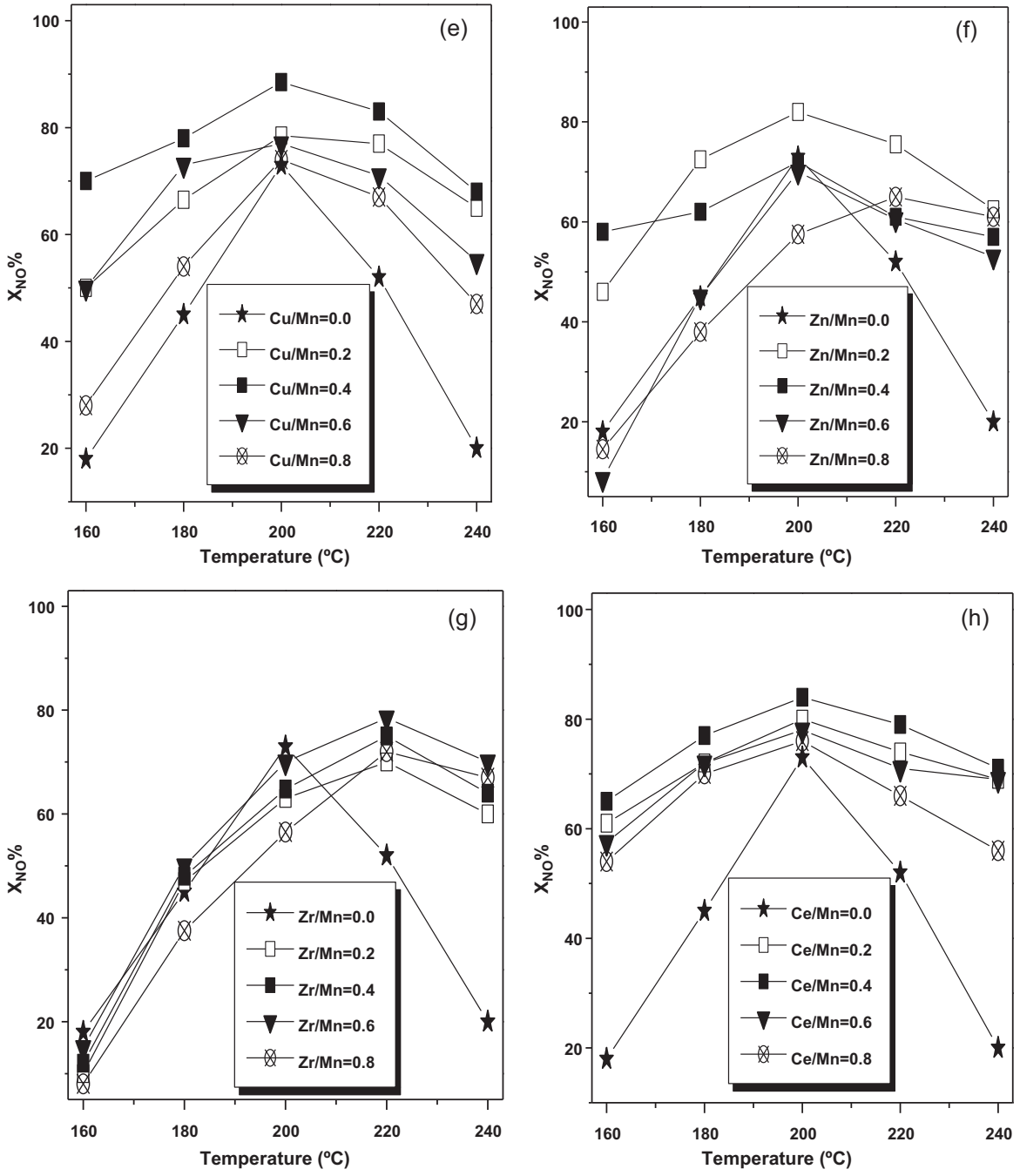

Fig. 5. *(Continued)*

lysts such as Mn–Zr(0)/TiO_2, Mn–Zr(0.2)/TiO_2, Mn–Zr(0.4)/TiO_2, Mn–Zr(0.6)/TiO_2, and Mn–Zr(0.8)/TiO_2 were also evaluated for the NH_3-SCR at low-temperatures. While, as expected the optimum temperature shifted to 220 °C and the promotion effect of zirconium is very low at below 220 °C as well as catalyst deactivated at above 220 °C. But the thermal stability of the Mn/TiO_2 catalyst improved greatly by the addition of zirconium oxide. From Fig. 5g, it can be suggested that among all the zirconia doped Mn/TiO_2 catalysts, optimal catalyst Mn–Zr(0.6)/TiO_2 showed good SCR activity and better stability.

Fig. 5h shows the NO conversions over the Mn/TiO_2 and Mn–Ce/TiO_2 catalysts in the temperature range of 160–240 °C with the function of various Ce/Mn atomic ratios. Mn–Ce(0.4)/TiO_2 and Mn–Ce(0.2)/TiO_2 catalysts showed higher NO conversions in the entire temperature range. These catalysts are more prominent below 200 °C, compared with other ceria doped Mn/TiO_2 (Ce/Mn = 0.6 and 0.8) catalysts. For instance, at 160 °C, Mn–Ce(0.4)/TiO_2 catalyst showed 65% NO conversion compared to Mn–Ce(0)/TiO_2 catalyst which showed only 18% NO conversion. The NO conversion increased with increase in the ceria content up to the 0.4 CeO_x/MnO_x ratio of the catalyst. The NO conversion decreased with further increase in the ceria content in the later (Mn–Ce(0.6)/TiO_2 and Mn–Ce(0.8)/TiO_2) catalysts. These results are in agreement with the reported literature, where the excess addition of manganese content to ceria, decreased the SCR activity at low-temperatures [17]. The SCR activity of all the ceria doped Mn/TiO_2 and Mn/TiO_2 catalysts dropped to the lower NO conversions at higher temperatures, it could be possibly due to sintering

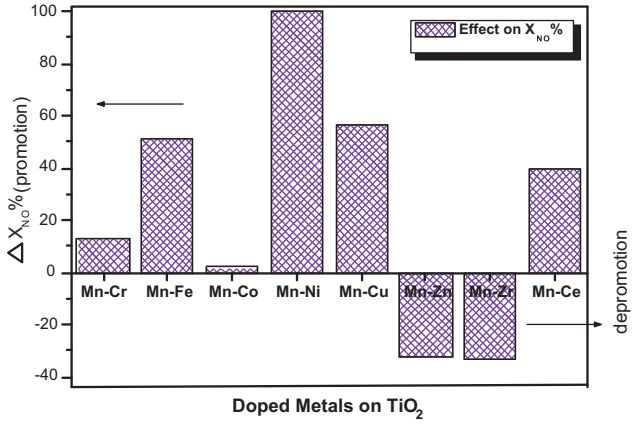

Fig. 6. Promotion effect of co-doped metals on Mn/TiO_2 in the NH_3-SCR reaction at 200 °C temperature; GHSV = 50,000 h^{-1}; feed: NO = 400 ppm, NH_3 = 400 ppm, O_2 = 2 vol%, He carrier gas, catalyst = 0.1 g, total flow = 140 mL min^{-1}. ΔX_{NO}% = promotional effect conversion of NO at 6 h on stream.

of the catalyst. However, SCR activity and stability of the Mn/TiO_2 catalysts improved by the addition of cerium oxide.

The promoting effect of co-doped metals was explained based on the difference in NO conversions of Mn–M′/TiO_2 and Mn/TiO_2 catalysts divided by the "total need of promotion to reach the maximum (100%) NO conversion" (Eq. (3)).

$$\Delta X_{NO}\% = \frac{(X_{NO}\%)_{Mn-M'} - (X_{NO}\%)_{Mn}}{100 - (X_{NO}\%)_{Mn}} \times 100 \quad (3)$$

The adequate enhancement in the NO conversion relative to the undoped Mn catalyst was tested with a high gas hourly space velocity (GHSV) 50,000 h^{-1}, at 200 °C temperature (Fig. 6). Relatively, among all the catalysts, nickel-doped titania-supported manganese catalyst showed 100% promotional effect on SCR activity of Mn/TiO_2. Except zinc-doped and zirconia-doped catalysts, all the other metals showed a positive impact on NO conversions of the Mn/TiO_2 catalyst. The SCR activity of titania-supported bimetallic catalysts and the promoting effect of co-doped metals at 200 °C temperature decreased in the following sequence: Mn–Ni/TiO_2 ≫ Mn–Cu/TiO_2 > Mn–Fe/TiO_2 > Mn–Ce/TiO_2 > Mn–Cr/TiO_2 ≫ Mn–Co/TiO_2 ⋙ Mn–Zn/TiO_2 ≅ Mn–Zr/TiO_2.

The effect of the co-doped metal on N_2 selectivity, and the NO conversions on continuous stream experiments were carried out in which the manganese was kept constant and by changing the co-doped metal in the sample. The NO conversions (at 1st hour and 6th hour on stream) and N_2 selectivity results are presented in Fig. 7. Mn–Ni/TiO_2 afforded highly impressive N_2 selectivity and catalytic activity relative to the other catalysts tested with 50,000 h^{-1} GHSV at 200 °C temperature. Mn–Cu/TiO_2 and Mn–Fe/TiO_2 catalysts also showed good activity and N_2 selectivity under these conditions.

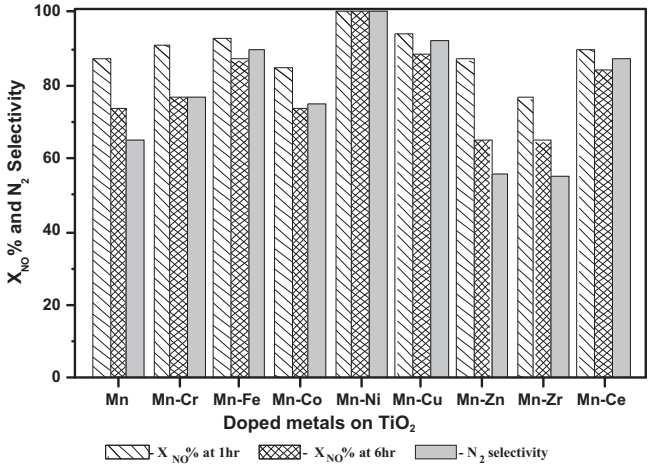

Fig. 7. N_2 selectivity and catalytic performance of Mn–M′/TiO_2 anatage catalysts: NH_3 = 400 ppm; NO = 400 ppm; O_2 = 2.0 vol%; GHSV = 50,000 h^{-1}; catalyst wt. = 0.1 g; reaction temperature = 200 °C.

4. Conclusions

The above data show quite clearly that samples with the same atomic composition can have very different properties, depending on the co-doped metals and on their chemical properties. The main differences were revealed by the combination of various characterization techniques employed. In our H_2-TPR studies, manganese reduction peak is shifted from 576 to 510 K, and the high temperature peak disappears. This increase in reducibility of manganese and absence of the high-temperature (736 K) peak suggested that the dominant phase is MnO_2 in Mn–Ni/TiO_2 catalyst. Our XPS results illustrated that the MnO_2 phase is extremely dominant over the Mn_2O_3 phase (Mn^{4+}/Mn^{3+} = 96%) in the Mn–Ni(0.4)/TiO_2 catalyst. The *in situ* NH_3-FTIR results revealed that the titania-supported manganese and manganese–nickel surface sites have only Lewis acidity. BET and pore volume measurements suggest high surface area and pore volume of the Mn–Ni/TiO_2 catalyst. All the experimental results showed that NO conversion, N_2 selectivity, broadening of temperature window and time on stream patterns of the catalyst are improved greatly by doping the Mn/TiO_2 catalyst with optimized (M′/Mn = 0.4) nickel. Among eight different types of co-dopants and five kind of M′/Mn atomic ratios in each type, Mn–Ni(0.4)/TiO_2 (Hombikat) catalyst is the best one for the low temperature SCR of NO with NH_3. This catalyst offers high NO conversion (100%), high N_2 selectivity (100%), and broadening of the temperature window with stable time on stream patterns.

Acknowledgement

The authors wish to acknowledge financial support from the National Science Foundation (Grant No. NSF-0828226).

References

[1] M. Kobayashi, R. Kuma, A. Morita, Catal. Lett. 112 (2006) 37–44.
[2] H. Schneider, M. Maciejewski, K. Köhler, A. Wokaun, A. Baiker, J. Catal. 157 (1995) 312.
[3] P.G. Smirniotis, D.A. Peña, B.S. Uphade, Angew. Chem. Int. Ed. 40 (2001) 2479–2482.
[4] F. Liu, H. He, C. Zhang, Z. Feng, L. Zheng, Y. Xie, T. Hu, Appl. Catal. B: Environ. 96 (2010) 408–420.
[5] D.A. Peña, B.S. Uphade, P.G. Smirniotis, J. Catal. 221 (2004) 421–431.
[6] P.M. Sreekanth, D.A. Peña, P.G. Smirniotis, Ind. Eng. Chem. Res. 45 (2006) 6444–6449.
[7] S. Cimino, S. Colonna, S. De Rossi, M. Faticanti, L. Lisi, I. Pettiti, P. Porta, J. Catal. 205 (2002) 309.
[8] A.M. Maltha, T.L.H. Favrem, H.F. Kist, A.P. Zuur, V. Ponec, J. Catal. 149 (1994) 364.
[9] R. Craciun, B. Nentwick, K. Hadjiivanov, H. Knözinger, Appl. Catal. A 243 (2003) 67.
[10] E.P. Reddy, E. Neeraja, M. Sergey, P. Boolchand, P.G. Smirniotis, Appl. Catal. B: Environ. 76 (2007) 123–134.
[11] T. Valdés-Solís, G. Marbán, A.B. Fuertes, Appl. Catal. B: Environ. 46 (2003) 261.
[12] S. Liang, X. Youjia, C. Qingqing, H. Bingqing, W. Chao, J. Guohua, Prog. Chem. 22 (2010) 1882.
[13] F. Kapteijn, L. Singoredjo, A. Andreini, Appl. Catal. B 3 (1994) 173–189.
[14] L. Ji, P.M. Sreekanth, P.G. Smirniotis, S.W. Thiel, N.G. Pinto, Energy Fuels 22 (2008) 2299–2306.
[15] G. Pechi, P. Reyes, T. Lopez, R. Gomez, A. Moreno, J.L.G. Fierro, J. Chem. Technol. Biotechnol. 77 (2002) 944.
[16] S.M. Saqer, D.I. Kondarides, X.E. Verykios, Appl. Catal. B: Environ. 108 (2011) 275–286.
[17] Z. Wu, B. Jiang, Y. Liu, Appl. Catal B: Environ. 79 (2008) 347–355.
[18] A. Rahman, M. Ahmed, Stud. Surf. Sci. Catal. 100 (1996) 419–426.
[19] P.M. Sreekanth, P.G. Smirniotis, Catal. Lett. 122 (2008) 37–42.
[20] M.M. Yung, E.M. Holmgreen, U.S. Ozkan, J. Catal. 247 (2007) 356.

[21] S.L. Sun, N. Tsubaki, K. Fujimoto, Appl. Catal. A: Gen. 202 (2000) 121.
[22] S. Bhatia, J. Beltramini, D.D. Do, Catal Today 7 (1990) 309.
[23] H.F.J. Van't Bilk, D.C. Koningsberger, R. Prins, J. Catal. 97 (1987) 210.
[24] F. Boccuzzi, A. Chiorino, G. Martra, M. Gargano, N. Ravasio, B. Carrozziniz, J. Catal. 165 (1997) 129–139.
[25] R. Zhang, A. Villanueva, H. Alamdari, S. Kaliaguine, Catal. Commun. 9 (2008) 111–116.
[26] D.J. Koh, J.S. Chung, Y.G. Kim, J.S. Lee, I.-S. Nam, S.H. Moon, J. Catal. 138 (1992) 630–639.
[27] H.C. Yao, Y.F. Yu-Yao, J. Catal. 86 (1984) 254.
[28] J.Z. Shyu, W.H. Weber, H.S. Gandhi, J. Phys. Chem. 92 (1988) 4964–4970.
[29] T. Yamaguchi, N. Ikeda, H. Hattori, K. Tanabe, J. Catal. 67 (1981) 324.
[30] D.A. Pena, B.S. Uphade, E.P. Reddy, P.G. Smirniotis, J. Phys. Chem. B 108 (2004) 9927–9936.
[31] G. Busca, L. Lietti, G. Ramis, G.F. Berti, Appl. Catal. B: Environ. 18 (1998) 1–36.
[32] F. Kapteijin, L. Singoredjo, M.V. Driel, A. Andreini, J.A. Moulijin, G. Ramis, G. Busca, J. Catal. 150 (1994) 105–116.
[33] H. Matralis, M. Ciardelli, M. Ruwet, P. Grange, J. Catal. 157 (1995) 523.
[34] G. Ramis, L. Yi, G. Busca, Catal. Today 28 (1996) 373.
[35] H. Knözinger, Adv. Catal. 25 (1976) 184.
[36] G. Busca, H. Saussey, O. Saur, J.C. Lavalley, V. Lorenzelli, Appl. Catal. 14 (1985) 245.
[37] G. Qi, R.T. Yang, J. Phys. Chem. B 108 (2004) 15738–15747.
[38] R.Y. Liu, Z. Wu, H. Wang, T. Gu, Chemosphere 78 (2010) 1160–1166.
[39] F.C. Buciuman, F. Patcas, T. Hahn, Chem. Eng. Proc. 38 (1999) 563–569.
[40] F. Kapteijn, L. Singoredjo, M. Vandriel, A. Andreini, J.A. Moulijn, G. Ramis, G. Busca, J. Catal. 150 (1994) 94.
[41] A. Machocki, T. Ioannides, B. Stasinska, W. Gac, G. Avgouropoulos, D. Delimaris, W. Grzegorczyk, S. Pasieczna, J. Catal. 227 (2004) 282–296.
[42] S. Ponce, M.A. Pena, J.L.G. Fierro, Appl. Catal. B 24 (2000) 193–205.
[43] C.D. Wagner, W.M. Riggs, L.E. Davis, J.F. Moulder, Handbook of X-ray Photoelectron Spectroscopy, Perkin-Elmer Corp., Physical Electronics Div., Eden Prairie, MN, 1979.
[44] R. Khodayari, Doctorial Dissertation, Lund Institute of Technology, Lund, Sweden, 2001, ISBN:91-7874-122-X.
[45] A.-C. Larsson, J. Einvall, A. Andersson, M. Sanati, Energy Fuels 20 (2006) 1398–1405.